ADVANCED MATERIALS
www.advmat.de

Mechanical Tolerance of Cascade Bioreactions via Adaptive Curvature Engineering for Epidermal Bioelectronics

Ting Wang, Qun-Li Lei, Ming Wang, Guoying Deng, Le Yang, Xijian Liu, Chunlin Li, Qi Wang, Zhihua Liu, Jianwu Wang, Zequn Cui, Kevin Goldio Utama, Ran Ni, and Xiaodong Chen**

Epidermal bioelectronics that can monitor human health status non-invasively and in real time are core to wearable healthcare equipment. Achieving mechanically tolerant surface bioreactions that convert biochemical information to detectable signals is crucial for obtaining high sensing fidelity. In this work, by combining simulations and experiments, a typical epidermal biosensor system is investigated based on a redox enzyme cascade reaction (RECR) comprising glucose oxidase/lactate oxidase enzymes and Prussian blue nanoparticles. Simulations reveal that strain-induced change in surface reactant flux is the key to the performance drop in traditional flat bioelectrodes. In contrast, wavy bioelectrodes capable of curvature adaptation maintain the reactant flux under strain, which preserves sensing fidelity. This rationale is experimentally proven by bioelectrodes with flat/wavy geometry under both static strain and dynamic stretching. When exposed to 50% strain, the signal fluctuations for wavy bioelectrodes are only 7.0% (4.9%) in detecting glucose (lactate), which are significantly lower than the 40.3% (51.8%) in flat bioelectrodes. Based on this wavy bioelectrode, a stable human epidermal metabolite biosensor insensitive to human gestures is further demonstrated. This mechanically tolerant biosensor based on adaptive curvature engineering provides a reliable bio/chemical-information monitoring platform for soft healthcare bioelectronics.

Epidermal bioelectronics open a window to monitor human health status via a non-invasive, real-time, and user-friendly way.[1–4] Recent years have witnessed their success in healthcare with increasing applications on epidermal electrophysiology and metabolites in perspiration.[5–8] One necessity as well as a challenge for epidermal bioelectronics is mechanical tolerance, that is, the ability to withstand mechanical deformations, which is a vital parameter to preserve signal fidelity in an inherent dynamic and stretchable epidermal system.[9–13] While mechanical tolerance has been demonstrated in monitoring electrophysiological signals,[14–16] it is more challenging to achieve mechanically tolerant biosensors that convert biochemical information to detectable signals, due to the difficulty in realizing invariance of surface bioreactions under deformation. Developing rigid biosensing area integrated with stretchable connectors has been proven as one way to circumvent this difficulty.[17–19] However, in order to realize intrinsically stretchable biosensors, it is necessary to achieve mechanical tolerance of surface bioreactions.

Redox enzymatic cascade reaction (RECR) comprises sequential enzyme-catalyzed chemical transformations.[20,21] In a single reaction vessel, the direct transportation of highly reactive intermediates between sequential enzymes suppresses side reactions and diffusional loss, resulting in high yields, cost effectiveness, and green synthesis.[22,23] Due to these advantages, RECR is widely used for epidermal biosensing, such as glucose biosensors based on glucose oxidase enzyme (GOx)/Prussian blue nanoparticles (PB NPs) couples, lactate biosensors based on lactate oxidase

Dr. T. Wang, Dr. M. Wang, Dr. X. Liu, Dr. Z. Liu, Dr. J. Wang, Dr. Z. Cui, K. G. Utama, Prof. X. Chen
Innovative Center for Flexible Devices (iFLEX)
Max Planck–NTU Joint Lab for Artificial Senses
School of Materials Science and Engineering
Nanyang Technological University
50 Nanyang Avenue, Singapore 639798, Singapore
E-mail: chenxd@ntu.edu.sg

The ORCID identification number(s) for the author(s) of this article can be found under https://doi.org/10.1002/adma.202000991.

DOI: 10.1002/adma.202000991

Dr. Q.-L. Lei, Prof. R. Ni
School of Chemical and Biomedical Engineering
Nanyang Technological University
62 Nanyang Drive, Singapore 637459, Singapore
E-mail: r.ni@ntu.edu.sg

Dr. G. Deng, C. Li, Q. Wang
Trauma & Emergency Center
Shanghai General Hospital
Shanghai Jiaotong University School of Medicine
100 Haining Road, Shanghai 200080, P. R. China

Dr. L. Yang
Institute of Materials Research and Engineering
Agency for Science Technology and Research (A*STAR)
2 Fusionopolis Way, Singapore 138634, Singapore

enzyme (LOx)/horseradish peroxidase (HRP) couples, and methyl salicylate biosensors based on salicylate hydroxylase/tyrosinase enzyme couples.[24–26] Therefore, it is important to have a fundamental understanding of how mechanical deformation affects RECR and develop a general strategy to achieve mechanically durable RECR.

In this work, through both simulations and experiments, we clarify that the increase in reactant (H_2O_2) transportation distance and its diffusion loss are two factors accounting for the cascade reaction efficiency drop in traditional stretchable flat electrodes. In contrast, wavy bioelectrodes with adaptive curvature exhibit stable performance resistant to both dynamic and static deformations. The wavy polydopamine(PDA)-polypyrrole(PPy)/enzymes/PB NPs/Au bioelectrodes in our experiments, prepared via a pre-stretching electrodeposition method, are further used as human epidermal biosensors. This biosensor exhibits stable metabolite monitoring when the human subject undergoes different movement gestures. A wide range of bioreactions can be incorporated into our mechanically tolerant epidermal biosensors based on adaptive curvature engineering, thus providing a durable and non-invasive platform for metabolite monitoring for soft healthcare bioelectronics.

The RECR we use in this work consists of two successive reactions. The first is the catalytic oxidation of glucose or lactate by GOx or LOx enzymes, simultaneously producing H_2O_2 in the presence of O_2. The second is the catalytic reduction of H_2O_2 by PB NPs, which transfers electrons to the electrode (**Figure 1**a).[27,28] These two kinds of catalysts are uniformly distributed on a flat or wavy stretchable bioelectrode. For a flat bioelectrode under strain, one would expect that the elongation

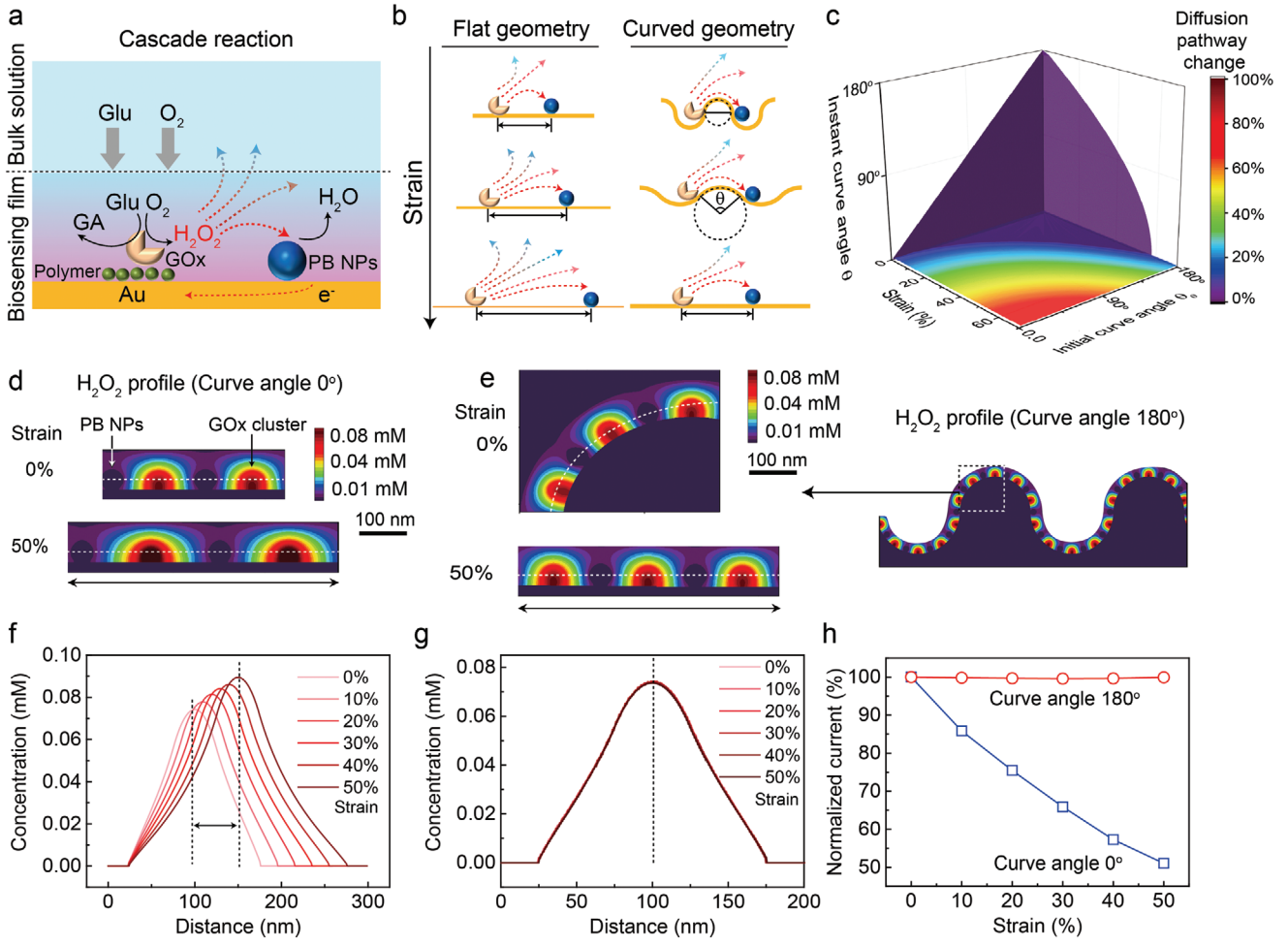

Figure 1. Theoretical studies of the mechanical tolerance of cascade reactions on bioelectrodes with different geometries. a) Scheme of cascade bioreactions on a film where glucose (Glu) and O_2 species diffusing from bulk solution are catalyzed by glucose oxidase enzyme (GOx) in the film, producing H_2O_2. The reduction of H_2O_2 is catalyzed by Prussian blue nanoparticles (PB NPs), which transfer electrons to the electrode at the applied potential. b) Reactant diffusion on flat and curved geometries when exposed to strain. The diffusion pathway is elongated on the flat bioelectrode, while that on the wavy bioelectrode remains the same due to the relaxation of curvature to accommodate the strains. The instant curve angle θ of wavy bioelectrode changes accordingly when exposed to strains. c) The dependence of diffusion pathway changes Δd (color) and instant curve angle θ (z axis) on the bioelectrode initial curve angle θ_0 and exposed strains Δl. d,e) Simulation results of equilibrium concentration profiles of H_2O_2 in the film for bioelectrodes with $\theta_0 = 0°$ and $\theta_0 = 180°$ under both 0% and 50% strain. f,g) Simulated H_2O_2 concentration profiles along the dashed line in (d) and (e), respectively, under different strain. Simulated H_2O_2 flux gradient decreases upon stretching for flat bioelectrodes with $\theta_0 = 0°$, while it remains stable for wavy bioelectrodes with $\theta_0 = 180°$. h) Simulated current signal decreases on flat bioelectrodes with $\theta_0 = 0°$, while signal keeps stable on wavy bioelectrodes with $\theta_0 = 180°$.

of elastomer lengthens the H_2O_2 diffusion pathway, that is, the surface distance along the bioelectrode between GOx and PB NPs (Figure 1b), which would reduce the accessibility of PB NPs to H_2O_2 and may ultimately influence the current response. While for a wavy bioelectrode under strain, its initial curvature can relax to accommodate the strain. As a result, the length of the diffusion pathway that approximates to the arch length remains almost unchanged (Figure 1b). When the wavy period is fixed (about 2 μm according to experimental data), the curvature of the surface can be represented by the instant curve angle θ. Theoretically, we obtain the change in diffusion pathway length Δd as a function of the strain and initial curve angle θ_0 based on simple geometry analysis (Equations (S1)–(S5) and Figure S1, Supporting Information).

$$\Delta d = \begin{cases} 0 & (\Delta l \le \Delta l^*) \\ (1+\Delta l)\dfrac{2}{\theta_0}\sin\left(\dfrac{\theta_0}{2}\right) - 1 & (\Delta l > \Delta l^*) \end{cases} \quad (1)$$

Here, Δl is the stretching ratio representing strain magnitude, which determines the θ through

$$\Delta l = \frac{\theta_0 \sin\left(\dfrac{\theta}{2}\right)}{\theta \sin\left(\dfrac{\theta_0}{2}\right)} - 1 \quad (2)$$

In Equation (1), $\Delta l^* = \dfrac{\theta_0}{2\sin\left(\dfrac{\theta_0}{2}\right)} - 1$ is the threshold strain, at which θ is zero. Figure 1c shows the change of diffusion pathway length Δd (color) and instant curve angle θ (z axis) as a function of strain (x axis) and initial curve angle θ_0 (y axis) according to Equations (1) and (2). Evidently, with increasing strain, pathway length remains unchanged as long as θ remains positive. Once the θ decreases to zero, further increasing the strain of electrodes leads to a growing diffusion pathway. This threshold strain Δl^* raises with increasing initial curvature. Thus, compared with flat bioelectrodes, wavy bioelectrodes with adaptive curvature can sustain much larger strain without changing the surface distance of the diffusion pathway.

To verify this conjecture and further explore the mass transportation and flux-limiting properties of RECR during stretching, we conduct simulations for both flat and wavy biosensors with different initial curvatures. Our simulation model relies on the following simplifications: the three free species, namely glucose, O_2, and H_2O_2, obey Fick's diffusion laws, and reactions among them are isothermal.[29–31] GOx and PB NPs, about 50 nm in size, are alternately and uniformly distributed on the film with separation distances of about 100 nm based on SEM images. 2D cross-section concentration profile is used to represent 3D concentration profile. Glucose and O_2 diffusing from the bulk solution are consumed at GOx, which produces H_2O_2 in situ. This reaction is modeled as a two-substrate Michaelis–Menten "ping-pong" type process. A similar model is applied for the H_2O_2 reduction at PB NP, which is found to be diffusion-limiting due to low concentrations of H_2O_2 in the film. The current signal reflects the reaction rate at PB NP. The whole process is described by the reaction-diffusion equations (S6)–(S8) in Supporting Information, which are integrated numerically to obtain the stable concentration profiles of glucose, O_2, and H_2O_2, and the current signal. The simulation details including all parameters used are given in Figure S2 and Table S1, Supporting Information.[30,32]

For both types of bioelectrodes, our simulation data shows high (low) H_2O_2 concentration near the GOx (PB NPs) region, since GOx (PB NPs) is the source (sink) for H_2O_2 (Figure 1d,e). Similarly, low concentrations of glucose and O_2 are found near GOx, which is the sink of the two species (Figure S3, Supporting Information). For flat bioelectrodes, upon stretching, the concentration profile of H_2O_2 becomes significantly more dispersed due to the increase in distance between the source and the sink (Figure 1d). Such stretching of the H_2O_2 profile upon increasing strain can be seen more clearly by the measured concentration along a contour line (white dashed line in Figure 1d) crossing the centers of PB NPs (Figure 1f). Similar behavior can also be found for glucose and O_2 (Figure S3, Supporting Information). These changes are accompanied by the current signal decrease upon stretching, showing a 50.4% drop when exposed to 50% strain (Figure 1h).

Two mechanisms are expected to account for such a performance drop on the flat bioelectrode. First, the detected current is proportional to the H_2O_2 reduction rate catalyzed by the PB NPs. Based on Fick's law of diffusion, the contact concentration gradient of H_2O_2 on the PB NPs surface determines the flux rate of H_2O_2 into the PB NPs region, which equals the reaction rate at equilibrium condition. The concentration gradient decays following a monotonic function of distance. Stretching increases the distance between the enzyme and PB NPs; hence, it also decreases the contact concentration gradient of H_2O_2 on PB NPs. Our simulation results show that along the contour line, the contact H_2O_2 concentration gradient indeed decreases upon stretching (Figure 1f). Second, H_2O_2 generated in the biolayer diffuses both toward the PB NPs and the bulk solutions.[33] Stretching increases the exposed areas of reaction interface to bulk solution. Since the H_2O_2 generation rate is insensitive to the strain (vide infra), this leads to more diffusion loss of H_2O_2 to the bulk and correspondingly less H_2O_2 consumption at the PB NPs due to the mass conservation.

As a comparison, we also conduct the simulations for wavy bioelectrodes with initial curvature of 180° (Figure 1e). In contrast with the flat bioelectrodes, we find the concentration profile to be only distorted but not dispersed upon stretching. In particular, the measured concentrations as well as their gradient along the contour line are strain-independent (Figure 1g). This leads to 99.7% preservation of initial current signal under as much as 50% strain (Figure 1h). Such a robust resistance to mechanical stretching is due to the aforementioned adaptive curvature mechanism, keeping the surface diffusion pathway unchanged and maintaining similar exposed surface area with equivalent H_2O_2 diffusion loss. Therefore, the adaptive curvature engineering provides an effective strategy to construct a mechanically tolerant RECR platform for epidermal biosensors.

The above theoretical prediction is experimentally validated with bioelectrodes of wavy geometry. Wavy bioelectrodes are prepared by a controllable pre-stretching electrodeposition method

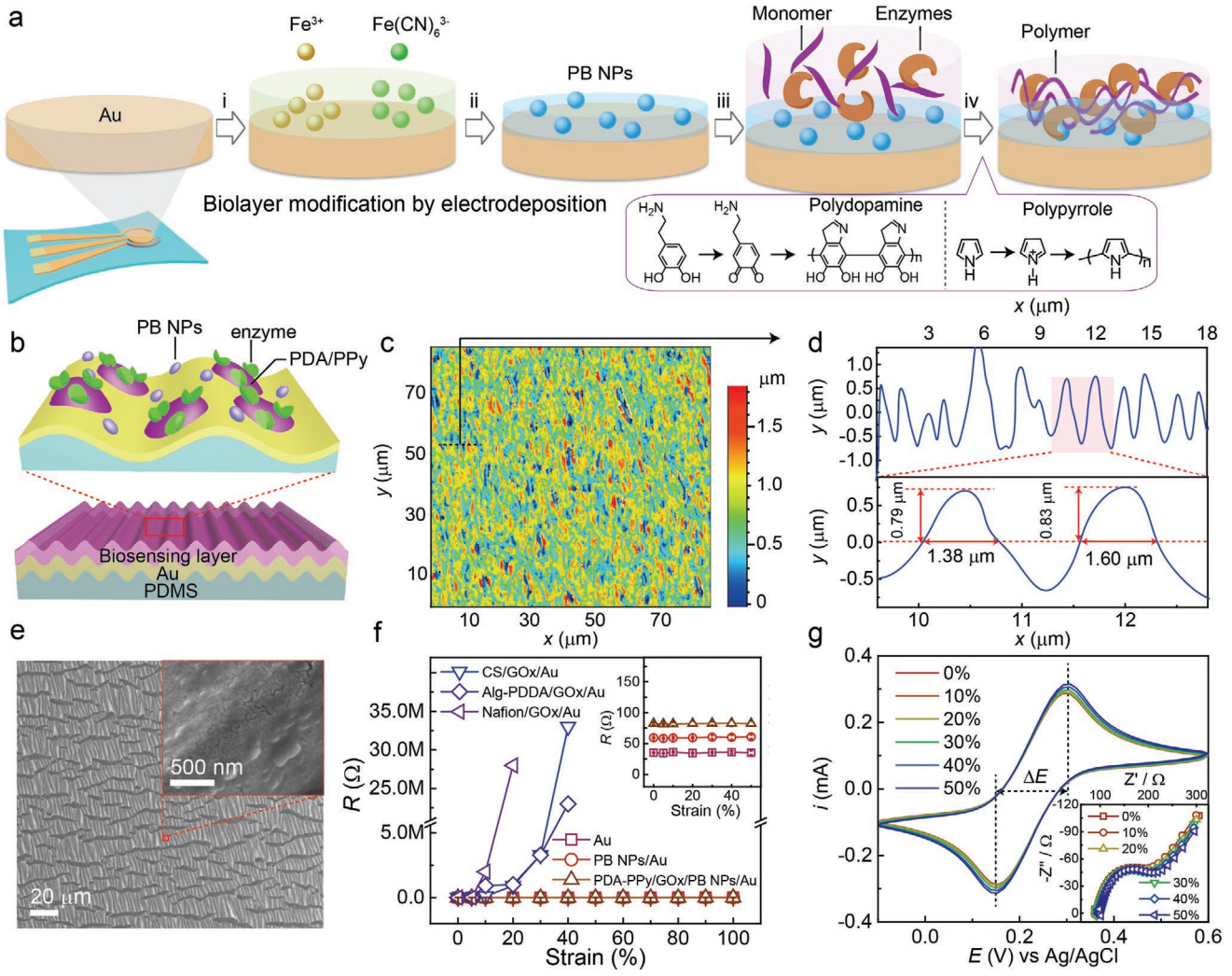

Figure 2. Preparation and characterization of wavy bioelectrodes prepared by the pre-stretching electrodeposition method. a) Biolayer modification of prestretched Au/PDMS electrode. (i,ii) PB NPs were electrodeposited on electrode via cyclic voltammetry in precursors. (iii,iv) Polymer with enzymes trapped were modified on electrode through electropolymerization of dopamine and pyrrole via cyclic voltammetry in monomer and enzyme mixture. b) Schematic structure of wavy bioelectrodes where enzymes and PB NPs are distributed on the wavy Au electrode. c,d) Profile of wavy bioelectrodes with wrinkles characterized by profilometry, which exhibit an average width of 1.5 ± 0.4 μm and height of 0.7 ± 0.2 μm. e) Morphology characterization of wavy PDA-PPy/GO_x/PB NPs/Au bioelectrodes. f) Resistance changes of wavy bioelectrodes prepared by electrodeposition (PB NPs/Au and PDA-PPy/GOx/PB NPs/Au) and drop-casting methods (chitosan [CS]/GOx/Au, alginic acid–poly(diallyldimethylammonium chloride) [Alg-PDDA]/GOx/Au and Nafion/GOx/Au). g) Electrochemical stability of wavy bioelectrodes by CV and EIS when exposed to different tensile strains.

(**Figure 2**a,b; Figure S4, Supporting Information). First, Au with pre-designed pattern and a thickness of 40 nm was thermally evaporated on poly(dimethylsiloxane) (PDMS) under 50% tensile state. PB NPs were then electrodeposited on the gold electrode using $K_3Fe(CN)_6$ and $FeCl_3$ in acid solutions. After that, GOx (LOx) were controllably immobilized via one-pot electropolymerization of dopamine (for higher enzyme adhesion) and pyrrole (for better conductivity) with the presence of enzymes in the solution. The mild polymerization condition in a neutral buffer solution helps to maintain enzyme activity.[34] During co-deposition of these monomers on electrodes, enzymes were captured in situ on the electrode. After biofunctionalization, the polymer/enzymes/PB NPs/Au/PDMS film was released from the 50% strain states. Due to the difference in interfacial mechanical properties,[35,36] uniform wrinkles are observed along the pre-stretching direction, as revealed by optical images (Figure S5, Supporting Information). These wrinkles can be viewed as wave structure with a periodic width of 1.5 ± 0.4 μm and height of 0.7 ± 0.2 μm as characterized by optical profilometry (Figure 2c,d). SEM images of the polymer/enzymes/PB NPs/Au/PDMS film also reveal wrinkled structures where particles are uniformly distributed on the curved surface (Figure 2e). These characterization results indicate wavy bioelectrodes have been fabricated by pre-stretching electrodeposition.

We then investigate the mechanical tolerance of wavy bioelectrodes for their electrical properties. Wavy bioelectrodes with width of 1 mm and length of 3 cm show stable conductivity under stretching (resistance changes of less than 20 Ω under 50% strain), comparable to bare gold electrodes (Figure 2f). $Fe(CN)_6^{3-}/Fe(CN)_6^{4-}$ is used as the redox probe to characterize

electrochemical activity via cyclic voltammetry (CV). The wavy bioelectrodes show typical redox peaks with peak-width variations of less than 6.3% when stretched up to 50% strain (Figure 2g). The electrochemical impedance spectroscopy (EIS) shows variation of 3.3% under 50% strain, indicating a stable electrochemical interface upon stretching (Figure 2g inset). We note that electrodeposition with good controllability and uniformity helps to preserve the conductive network of thin gold film compared to drip-dry modification methods, as seen from the large resistance changes under stretching for chitosan/GOx/Au, alginic acid–poly(diallyldimethylammonium chloride)/GOx/Au, and Nafion/GOx/Au electrodes (Figure 2f; Figure S6, Supporting Information). Detailed descriptions are given in Supporting Information.

Before testing the mechanical tolerance of biosensors, the immobilization matrix has been optimized by tuning the precursor composition, namely dopamine (DA) and pyrrole (Py), to maximize their full potential for biosensing performance. The mussel-inspired DA with high binding strength to biomolecules and metals allows for high enzyme-loading and good adhesion of the biolayer to the curved gold surface.[37,38] Increasing the DA monomer component therefore confers a higher adhesive function to the polymer, which contributes to better enzyme-loading (**Figure 3**c). Meanwhile Py helps to

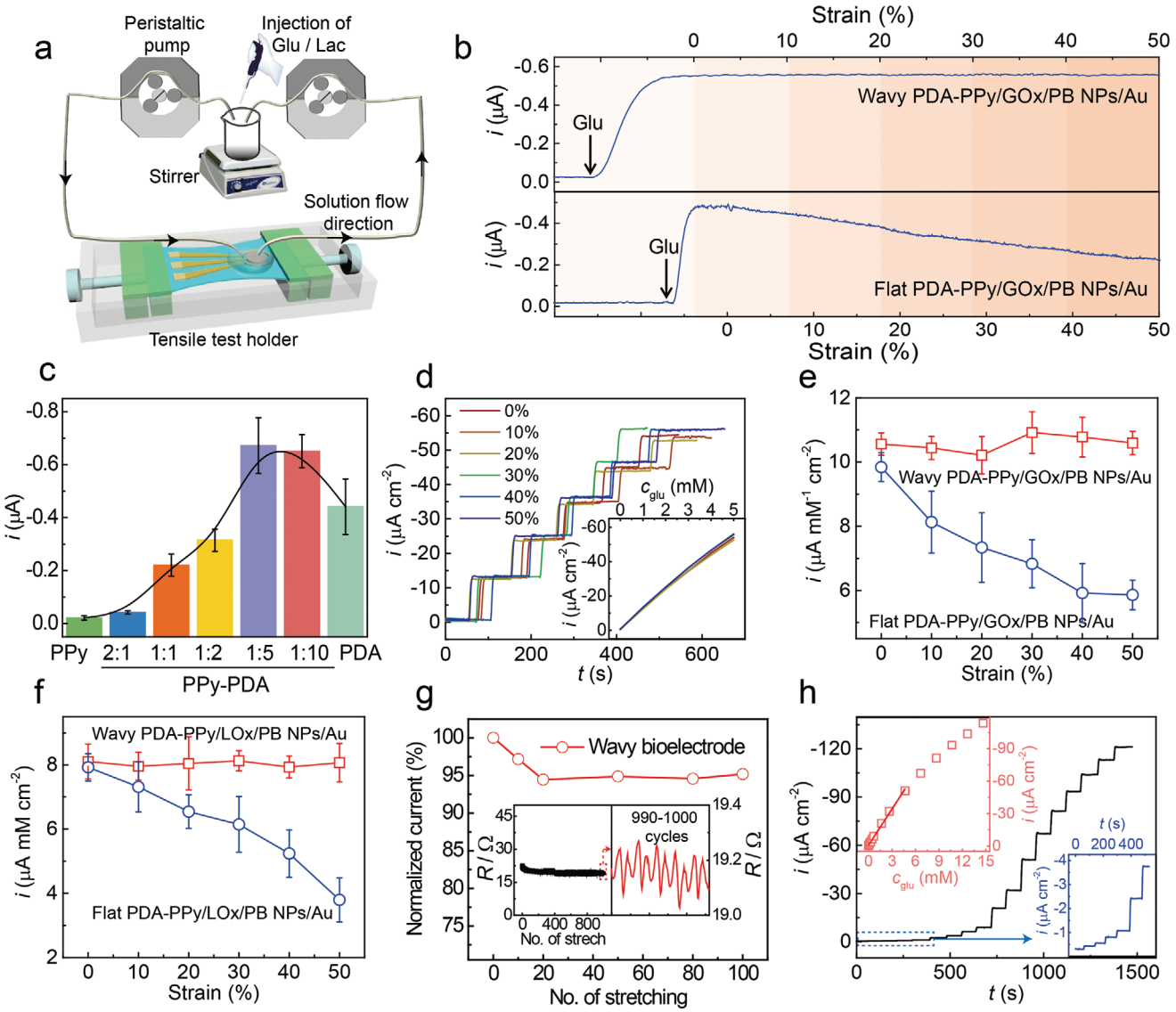

Figure 3. Experimental evidence of mechanical tolerance of wavy PDA-PPy/GOx/PB NPs/Au bioelectrodes. a) Experimental setup for metabolite sensing under dynamic and static tensile states. b) Stable biosensing performance of a wavy bioelectrode compared with the performance drop for a flat bioelectrode under dynamic stretching. c) The optimization of PPy to PDA ratio for optimal biosensing performance. d) Steady response current of wavy bioelectrodes under different static tensile states. Corresponding calibration curve is given in the inset. e) The biosensing sensitivity of wavy and flat glucose biosensors when exposed to different strain. f) The biosensing sensitivity of wavy and flat lactate biosensors when exposed to different strains. g) The robustness of biosensing performance and the conductivity (inset) of wavy biosensors after repeated stretching. h) Linear detection range of wavy glucose biosensors (concentration range from 5 μM to 6 mM).

enhance the conductivity of biolayer.[39,40] An optimal Py component in the polymer helps to enhance film conductivity, as confirmed by the EIS curves (Figure S7, Supporting Information). Hence, a biolayer prepared with a Py:DA molar ratio of 1:5 ($PPy\text{-}PDA_{1:5}$) has been found as the optimal bio-matrix for biosensors.

The mechanical tolerance of bioelectrodes has been measured by dynamic and static tensile testing. The setup includes two peristaltic pumps to keep the cyclic fluidic flow on the bioelectrodes and a stretching holder to apply the strain (Figure 3a) (setup details given in Supporting information). After injecting glucose/lactate in the beaker under stirring, the glucose/lactate solution flows to the biosensor fixed on the stretching holder. With the injection of 0.5 mM glucose, both wavy and flat biosensors show increase in steady currents, confirming the capability of glucose sensing based on cascade GOx and PB NPs couples (Figure 3b). Dynamical strain with stretching rate of 10% per minute is then applied. The current response of the flat biosensor shows a prominent decrease of 53.7% while that of the wavy biosensors shows negligible fluctuations within 5% (Figure 3b).

We further evaluate the response of biosensors with successive injection of glucose under different static stretching states, and steady current curves are presented in Figure 3d. When gradually increasing the strain to 50% with 10% strain increment each time, the wavy biosensors show comparable steady current curves with sensitivity variations within 7.0%. In contrast, flat biosensors show a current drop of 40.3% when strained up to 50% (Figure 3e). To further prove the generality of wavy biolayer strategy, wavy lactate biosensors also exhibit stable sensitivity with variations of 4.9% in current response, compared to flat biosensors with a current drop of 51.8% when exposed to 50% strain (Figure 3f). Both dynamic and static tensile testing validate the mechanical tolerance of wavy biosensors. Moreover, biosensors can sustain repeated stretching, as evident in their stable biosensing performance (variations of less than 7.4%) even after 100 stretching cycles with 50% strain (Figure 3g). Hence, wavy bioelectrodes exhibit stable sensing performance resistant to dynamic, static, and repeated stretching conditions.

The above experimental results are in good accordance with simulation prediction. For traditional flat bioelectrodes, stretching elongates the distance between the enzyme and PB NPs, which lengthens the H_2O_2 diffusion pathway and increases the diffusion loss of H_2O_2, finally leading to current decrease. In comparison, wavy bioelectrodes can relax the instant curvature to accommodate the strain and avoid these adverse effects on cascade bioreactions, contributing to mechanically-tolerant RECR.

To further corroborate this, we design a colorimetric biosensing system where localized H_2O_2 diffusion is avoided. In this system, GOx is immobilized in the film while HRP is dispersed in the solution. *o*-dianisidine in the solution is used as the colorimetric indicator. Here, H_2O_2 produced in the film diffuses to the solution, where it is reduced catalytically by HRP, producing oxidized *o*-dianisidine with colorimetric response. The colorimetric reaction mechanism and testing procedures are similar to literature,[41] as explained in Supporting Information. Vigorous stirring enhances the diffusion process and homogeneity of the solution. We find that the colorimetric responses of both flat and wavy biosensors are not affected by the tensile state (Figure S8, Supporting Information). This suggests that, in the colorimetric system, as the biosensing film is fully immersed in the solution, strain has little effect on the distance between GOx on the film and HRP in the solution, thus preventing a decrease in cascade efficiency. Besides, strain-insensitive colorimetric response indicates that H_2O_2 generation is insensitive to the strain. Comparison of electrochemical and colorimetric systems indicates that invariance of reactant transfer pathway is an important factor to preserve cascade bioreaction efficiency.

We note that conductivity also influences the electrochemical biosensing performance.[11,18] To investigate this, we use a rheostat in series with the biosensor to quantitatively evaluate the impact of the electrode resistance on biosensing performance. We observe that a gradual increase of rheostat resistance leads to performance decrease (Figure S9a, Supporting Information). Based on the fitted curve (Figure S9b, Supporting Information), we estimate a resistance change of 5 kΩ ± 0.5 kΩ for flat electrode under 50% strain (Figure S10, Supporting Information) would account for 15% to 20% current decrease. Therefore, apart from reactant transfer, conductivity is another factor that results in performance decrease in flat bioelectrodes. In contrast, wavy biosensors show robust conductive networks with negligible resistance of less than 20 Ω upon 50% strain (Figure 2f) and can sustain 1000 stretching cycles (Figure 3g inset). Therefore, wavy bioelectrodes maintain stable cascade bioreaction efficiency and robust electrochemical interfacial conductivity under strain. These two advantages synergistically contribute to a durable RECR platform for a wide range of applications involving mechanical deformation such as epidermal bioelectronics.

Finally, biosensors are demonstrated in human epidermal metabolite sensing. Steady current testing shows that wavy bioelectrodes exhibit a linear detection range for glucose from 5 μM to 6 mM (Figure 3h) with a detection limit of 1 μM, useful for detecting perspiration glucose with a physiological range of 10–200 μM and blood glucose up to 4–6 mM.[42] The reliability of our biosensors was further confirmed by no significant difference ($p > 0.05$) when comparing our results with that of commercial glucose meter when testing 4 mM glucose in buffer solution (Figure S11, Supporting Information). Similarly, we obtain lactate biosensors with a linear detection range from 1 to 660 μM by using LOx as the biosensing molecules (Figure S12, Supporting Information). As a proof of concept, the biosensing device is attached to a person's neck, a sweat-producing area (**Figure 4**a). The biosensing device comprises an electrode layer on elastomer, polymer/enzyme/PB NPs layer, parafilm for insulation, and a silk film for adhesion. Ag/AgCl reference electrodes with stable potential under stretching have been prepared by electric-chlorination of wavy silver electrodes with optimized parameters, as described in Figure S13, Supporting Information. To eliminate the difference between PBS solution and real sweat, we use sweat as the buffer solution to obtain calibration working curves for sweat glucose testing. As seen from the chronoamperometric response, the wavy PDA-PPy/GOx/PB NPs/Au shows a linear detection range from 5 to 1000 μM based on a steady current at 100 s (Figure 4b).

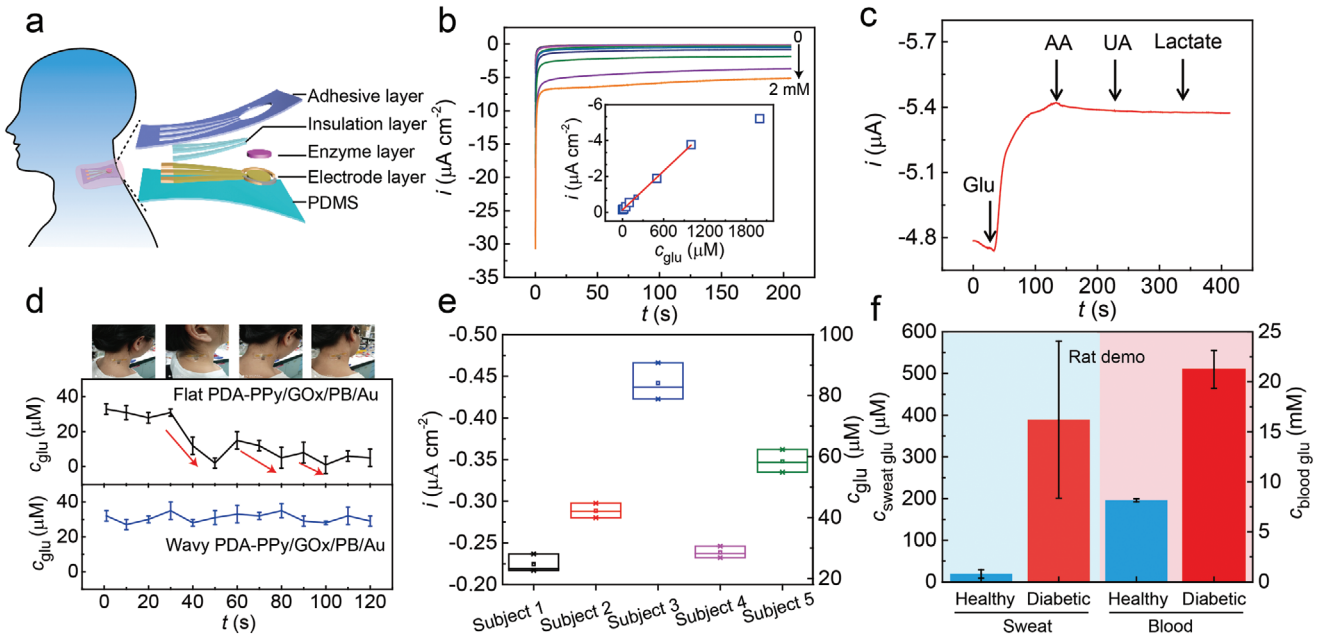

Figure 4. Demonstration of epidermal metabolite biosensor by using wavy bioelectrodes. a) The configuration of epidermal biosensors which comprise adhesion, insulation, enzyme, electrode, and PDMS layers. b) Glucose biosensing performance and its calibrated working curve using healthy sweat as the buffer solution. The arrow indicates concentration increment from 0 to 2 mM. c) The selectivity of wavy PDA-PPy/GOx/PB NPs/Au bioelectrode tested with the addition of 500 μM glucose, 1 mM of ascorbic acid (AA), uric acid (UA), and lactate in sequence under a potential of −0.05 V versus Ag/AgCl. d) Durability of wavy PDA-PPy/GOx/PB NPs/Au biosensors on epidermis when the subject changed different gestures compared with gesture-induced large signal fluctuation of flat biosensors. e) The glucose concentration in the perspiration of different healthy subjects measured by wavy bioelectrodes based on three parallel experiments. f) The tested glucose concentration in the stimulated sweat of diabetic and healthy rats, which shows similar trends as blood glucose.

The responsive range covers a significant concentration range of glucose in perspiration for monitoring diabetes. The selectivity of sweat sensors is verified by the negligible response of non-target metabolites, ensuring low interference from other metabolites in sweat (Figure 4c). Sweat glucose testing results show that glucose concentrations in the perspiration of five healthy persons are in the range of 20 to 100 μM (Figure 4e), which is in accordance with reported ranges in the literature,[42] and when the subject moves into different gestures, the wavy biosensor shows stable biosensing data while the flat biosensors show significant performance variations, confirming the mechanical tolerance feature of the wavy biosensors (Figure 4d). To test the feasibility of sensing sweat glucose for diabetes monitoring, we use healthy and diabetic rats by comparing the concentration trends between their blood and sweat glucose, as described in Supporting Information. The sweat glucose in the diabetic rat shows a significantly higher concentration than that of the healthy rat, corresponding to blood glucose concentration trends (Figure 4f) in diabetic (400–600 mg dL^{-1}) rats, and ≤150 mg dL^{-1} in healthy rats.[43] All these results validate the reliability of wavy PDA-PPy/GOx/PB NPs/Au bioelectrodes as a mechanically tolerant biosensing platform, which can be used for real-time, non-invasive, and continuous epidermal diabetes monitoring.

In short, through both theoretical simulation and experimental verification, our research shows that the adaptive curvature engineering can be utilized to achieve the mechanical tolerance of redox enzyme cascade reaction. Simulation reveals that the elongation of reactant transfer pathway and increase of reactant diffusion loss are key reasons for the performance drop in the flat bioelectrodes under stretching. In contrast, wavy bioelectrodes are capable of relaxing curvatures to maintain reactant transfer pathways as well as diffusion loss, preserving the performance under strain. This is rationalized in wavy PDA-PPy/GOx/PB NPs/Au biosensors prepared by a one-pot pre-stretching electrodeposition method. The wavy bioelectrodes sustain both static strain and dynamic stretching, exhibiting only 7.0% biosensing performance variations for glucose and 4.9% for lactate when exposed to 50% strain. In comparison, flat bioelectrodes exhibit a performance drop of 40.3% (glucose) and 51.8% (lactate) under the same 50% strain. Finally, wavy bioelectrodes with stable biosensing performance have been demonstrated for sweat metabolite monitoring on human neck with different movement gestures. Such epidermal biosensors in principle can be incorporated with many other bioreactions, providing a reliable platform for durable and non-invasive perception of human health status.

Supporting Information

Supporting Information is available from the Wiley Online Library or from the author.

Acknowledgements

T. W. and Q.-L. L. contributed equally to this work. The authors thank the financial support from the Agency for Science, Technology and Research (A*STAR) under its AME Programmatic Funding Scheme

(Project #A18A1b0045) Cyber-Physiochemical Interfaces (CPI) Programme, the National Research Foundation (NRF), Prime Minister's office, Singapore under its NRF Investigatorship (NRF-NRFI2017-07), Singapore Ministry of Education (MOE2017-T2-2-107), the Singapore Ministry of Education through the Academic Tier 1 Research Fund (M4011873.120), the Nanyang Technological University Start-Up Grant (NTU-SUG: M4081781.120), and the A*STAR Advanced Manufacturing and Engineering Young Individual Research Grant (A1784C0018). The tests on human skin were approved by the Institute of Review Board, Nanyang Technological University (approval number: IRB-2017-08-035-01). Informed consent from all volunteers was obtained prior to the experiments. The animal experiment was approved by the School of Medicine Animal Care and Use Committee, Shanghai Jiaotong University (approved number: A-2018-010).

Conflict of Interest

The authors declare no conflict of interest.

Keywords

cascade reaction, epidermal biosensors, mechanical tolerance, metabolite monitoring, soft bioelectronics

Received: February 11, 2020
Revised: March 19, 2020
Published online:

[1] W. Gao, H. Ota, D. Kiriya, K. Takei, A. Javey, *Acc. Chem. Res.* **2019**, *52*, 523.
[2] J. Rogers, Z. Bao, T.-W. Lee, *Acc. Chem. Res.* **2019**, *52*, 521.
[3] C. S. Wood, M. R. Thomas, J. Budd, T. P. Mashamba-Thompson, K. Herbst, D. Pillay, R. W. Peeling, A. M. Johnson, R. A. McKendry, M. M. Stevens, *Nature* **2019**, *566*, 467.
[4] T. Wang, M. Wang, L. Yang, Z. Li, X. J. Loh, X. Chen, *Adv. Mater.* **2020**, *32*, 1905522.
[5] W. Gao, S. Emaminejad, H. Y. Y. Nyein, S. Challa, K. Chen, A. Peck, H. M. Fahad, H. Ota, H. Shiraki, D. Kiriya, *Nature* **2016**, *529*, 509.
[6] M. Bariya, H. Y. Y. Nyein, A. Javey, *Nat. Electron.* **2018**, *1*, 160.
[7] S. Emaminejad, W. Gao, E. Wu, Z. A. Davies, H. Y. Y. Nyein, S. Challa, S. P. Ryan, H. M. Fahad, K. Chen, Z. Shahpar, *Proc. Natl. Acad. Sci. USA* **2017**, *114*, 4625.
[8] Y. Yang, W. Gao, *Chem. Soc. Rev.* **2019**, *48*, 12280.
[9] R. C. Webb, A. P. Bonifas, A. Behnaz, Y. Zhang, K. J. Yu, H. Cheng, M. Shi, Z. Bian, Z. Liu, Y.-S. Kim, *Nat. Mater.* **2013**, *12*, 938.
[10] A. Koh, D. Kang, Y. Xue, S. Lee, R. M. Pielak, J. Kim, T. Hwang, S. Min, A. Banks, P. Bastien, *Sci. Transl. Med.* **2016**, *8*, 366ra165.
[11] X. Chen, *Small Methods* **2017**, *1*, 1600029.
[12] G. Chen, N. Matsuhisa, Z. Liu, D. Qi, P. Cai, Y. Jiang, C. Wan, Y. Cui, W. R. Leow, Z. Liu, S. Gong, K.-Q. Zhang, Y. Cheng, X. Chen, *Adv. Mater.* **2018**, *30*, 1800129.
[13] S. Stauss, I. Honma, *Bull. Chem. Soc. Jpn.* **2018**, *91*, 492.
[14] D. Qi, Z. Liu, Y. Liu, Y. Jiang, W. R. Leow, M. Pal, S. Pan, H. Yang, Y. Wang, X. Zhang, J. Yu, B. Li, Z. Yu, W. Wang, X. Chen, *Adv. Mater.* **2017**, *29*, 1702800.
[15] D.-H. Kim, N. Lu, R. Ma, Y.-S. Kim, R.-H. Kim, S. Wang, J. Wu, S. M. Won, H. Tao, A. Islam, *Science* **2011**, *333*, 838.
[16] Y. Zhang, T. H. Tao, *Adv. Mater.* **2019**, *31*, 1905767.
[17] H. Lee, T. K. Choi, Y. B. Lee, H. R. Cho, R. Ghaffari, L. Wang, H. J. Choi, T. D. Chung, N. Lu, T. Hyeon, *Nat. Nanotechnol.* **2016**, *11*, 566.
[18] A. J. Bandodkar, R. Nuñez-Flores, W. Jia, J. Wang, *Adv. Mater.* **2015**, *27*, 3060.
[19] Q. Zhai, S. Gong, Y. Wang, Q. Lyu, Y. Liu, Y. Ling, J. Wang, G. P. Simon, W. Cheng, *ACS Appl. Mater. Interfaces* **2019**, *11*, 9724.
[20] J. M. Sperl, V. Sieber, *ACS Catal.* **2018**, *8*, 2385.
[21] T. A. Ngo, E. Nakata, M. Saimura, T. Morii, *J. Am. Chem. Soc.* **2016**, *138*, 3012.
[22] J. H. Schrittwieser, S. Velikogne, M. l. Hall, W. Kroutil, *Chem. Rev.* **2018**, *118*, 270.
[23] K. C. Nicolaou, J. S. Chen, *Chem. Soc. Rev.* **2009**, *38*, 2993.
[24] K. S. Rabe, J. Müller, M. Skoupi, C. M. Niemeyer, *Angew. Chem., Int. Ed.* **2017**, *56*, 13574.
[25] J. Fu, Y. R. Yang, A. Johnson-Buck, M. Liu, Y. Liu, N. G. Walter, N. W. Woodbury, H. Yan, *Nat. Nanotechnol.* **2014**, *9*, 531.
[26] T. Wang, Y. Fu, L. Bu, C. Qin, Y. Meng, C. Chen, M. Ma, Q. Xie, S. Yao, *J. Phys. Chem. C* **2012**, *116*, 20908.
[27] D. Grieshaber, R. MacKenzie, J. Voeroes, E. Reimhult, *Sensors* **2008**, *8*, 1400.
[28] T. Wang, Y. Fu, L. Chai, L. Chao, L. Bu, Y. Meng, C. Chen, M. Ma, Q. Xie, S. Yao, *Chem. - Eur. J.* **2014**, *20*, 2623.
[29] V. Ašeris, R. Baronas, J. Kulys, *J. Electroanal. Chem.* **2012**, *685*, 63.
[30] R. A. Croce Jr., S. Vaddiraju, A. Legassey, F. Papadimitrakopoulos, F. C. Jain, *Int. J. High Speed Electron. Syst.* **2015**, *24*, 1550012.
[31] J. Y. Wu, H. S. Weng, *Biotechnol. Bioeng.* **1989**, *33*, 415.
[32] J. Singh, N. Verma, *Adv. Appl. Sci. Res.* **2013**, *4*, 250.
[33] S. Vaddiraju, D. Burgess, F. Jain, F. Papadimitrakopoulos, *Biosens. Bioelectron.* **2009**, *24*, 1557.
[34] Y. Fu, P. Li, Q. Xie, X. Xu, L. Lei, C. Chen, C. Zou, W. Deng, S. Yao, *Adv. Funct. Mater.* **2009**, *19*, 1784.
[35] G. Cantarella, C. Vogt, R. Hopf, N. Münzenrieder, P. Andrianakis, L. Petti, A. Daus, S. Knobelspies, L. Büthe, G. Tröster, *ACS Appl. Mater. Interfaces* **2017**, *9*, 28750.
[36] D.-H. Kim, J.-H. Ahn, W. M. Choi, H.-S. Kim, T.-H. Kim, J. Song, Y. Y. Huang, Z. Liu, C. Lu, J. A. Rogers, *Science* **2008**, *320*, 507.
[37] W. Yang, C. Liu, Y. Chen, *Langmuir* **2018**, *34*, 3565.
[38] Y. Liu, K. Ai, L. Lu, *Chem. Rev.* **2014**, *114*, 5057.
[39] M. H. Naveen, N. G. Gurudatt, Y.-B. Shim, *Appl. Mater. Today* **2017**, *9*, 419.
[40] S. Inal, J. Rivnay, A.-O. Suiu, G. G. Malliaras, I. McCulloch, *Acc. Chem. Res.* **2018**, *51*, 1368.
[41] C. Dhand, G. Sumana, M. Datta, B. Malhotra, *Thin Solid Films* **2010**, *519*, 1145.
[42] D. Bruen, C. Delaney, L. Florea, D. Diamond, *Sensors* **2017**, *17*, 1866.
[43] G. A. Behr, E. G. Da Silva, A. R. Ferreira, C. T. S. Cerski, F. Dal-Pizzol, J. C. F. Moreira, *Fundam. Clin. Pharmacol.* **2008**, *22*, 657.

